Electronic Supplementary Information (ESI)

One-step solid-state pyrolysis of bio-wastes to synthesize multi-hierarchical porous carbon for ultra-long life supercapacitors

Min Fu,[a] Jintao Huang,[b,c*] Simin Feng,[d] Tianyi Zhang,[e] Peng-Cheng Qian,[f,*] Wai-Yeung Wong[c,*]

[a] College of Chemical and Biological Engineering, Shandong University of Science and Technology, Qingdao 266590, China

[b] Department of Polymeric Materials and Engineering, School of Materials and Energy, Guangdong University of Technology, Guangzhou, 510006, China

[c] Department of Applied Biology and Chemical Technology and Research Institute for Smart Energy, The Hong Kong Polytechnic University, Hung Hom, Hong Kong, China

[d] i-Lab, Key Laboratory of Multifunctional Nanomaterials and Smart Systems, Suzhou Institute of Nano-Tech and Nano-Bionics, Chinese Academy of Sciences, Suzhou, 215123, China

[e] Department of Materials Science and Engineering, The Pennsylvania State University, University Park, PA 16802, USA

[f] Key Laboratory of Environmental Functional Materials Technology and Application of Wenzhou City, Institute of New Materials & Industry, College of Chemistry & Materials Engineering, Wenzhou University, Wenzhou 325035, China

Corresponding authors: jintao.huang@gdut.edu.cn (Jintao Huang), wai-yeung.wong@polyu.edu.hk (Wai-Yeung Wong), pcqian@sina.com (Peng-Cheng Qian)

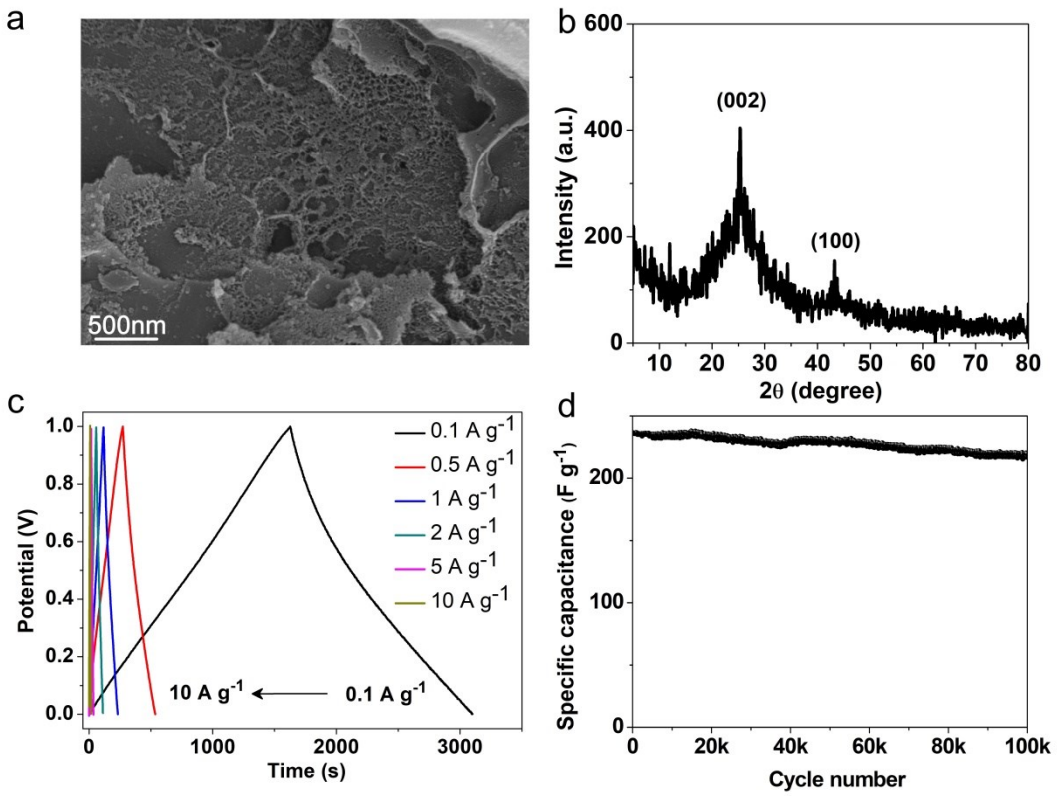

Figure S1 (a) SEM image and (b) XRD pattern of shrimp shell derived porous carbon; (c) GCD curves and (d) cyclic performances of the corresponding supercapacitor.

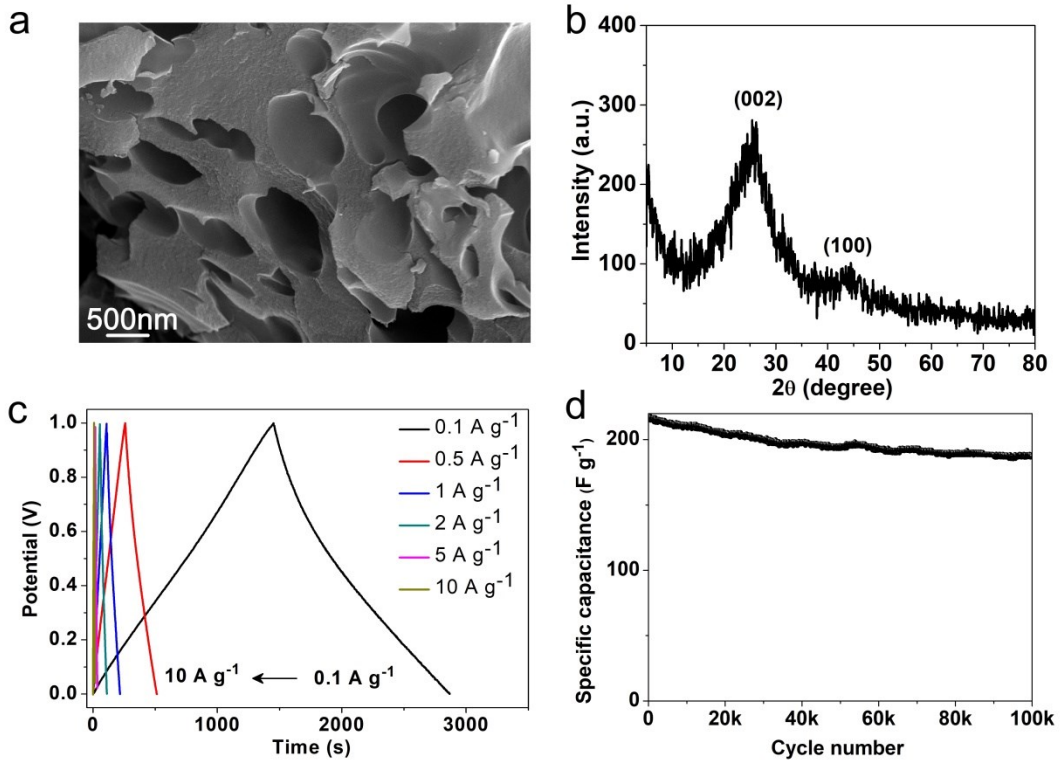

Figure S2 (a) SEM image and (b) XRD pattern of chestnut shell derived porous carbon; (c) GCD curves and (d) cyclic performances of the corresponding supercapacitor.

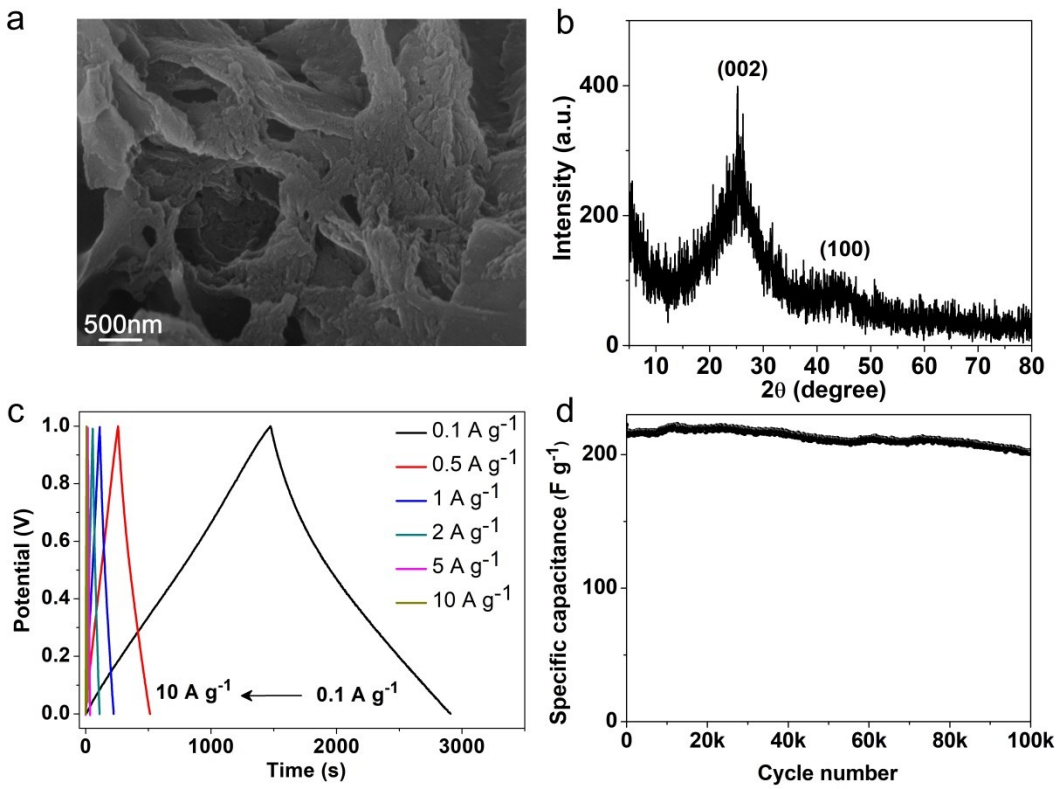

Figure S3 (a) SEM image and (b) XRD pattern of lamb bone derived porous carbon; (c) GCD curves and (d) cyclic performances of the corresponding supercapacitor.

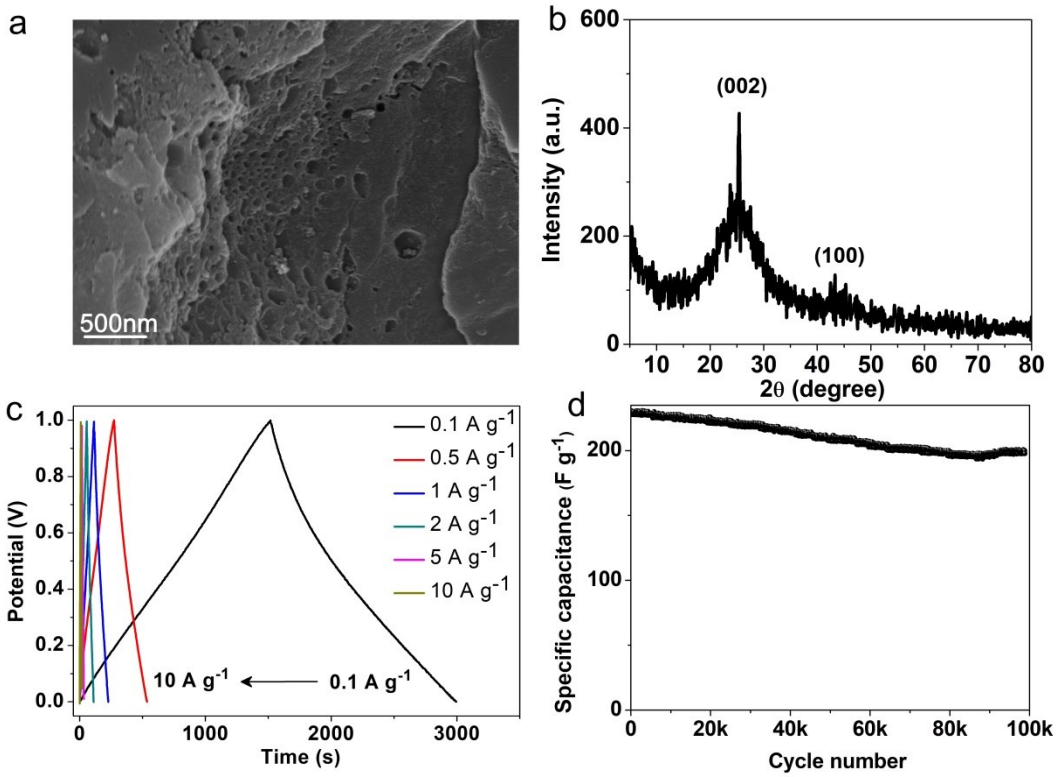

Figure S4 (a) SEM image and (b) XRD pattern of pomelopeel derived porous carbon; (c) GCD curves and (d) cyclic performances of the corresponding supercapacitor.

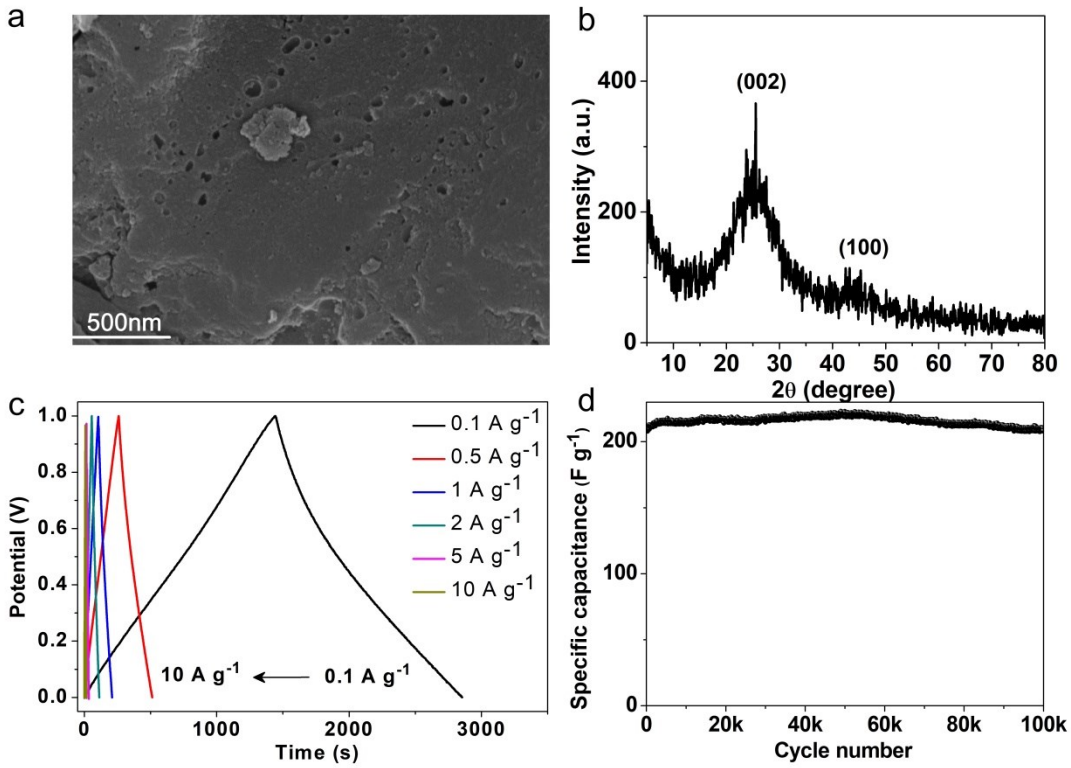

Figure S5 (a) SEM image and (b) XRD pattern of peanut shell derived porous carbon; (c) GCD curves and (d) cyclic performances of the corresponding supercapacitor.

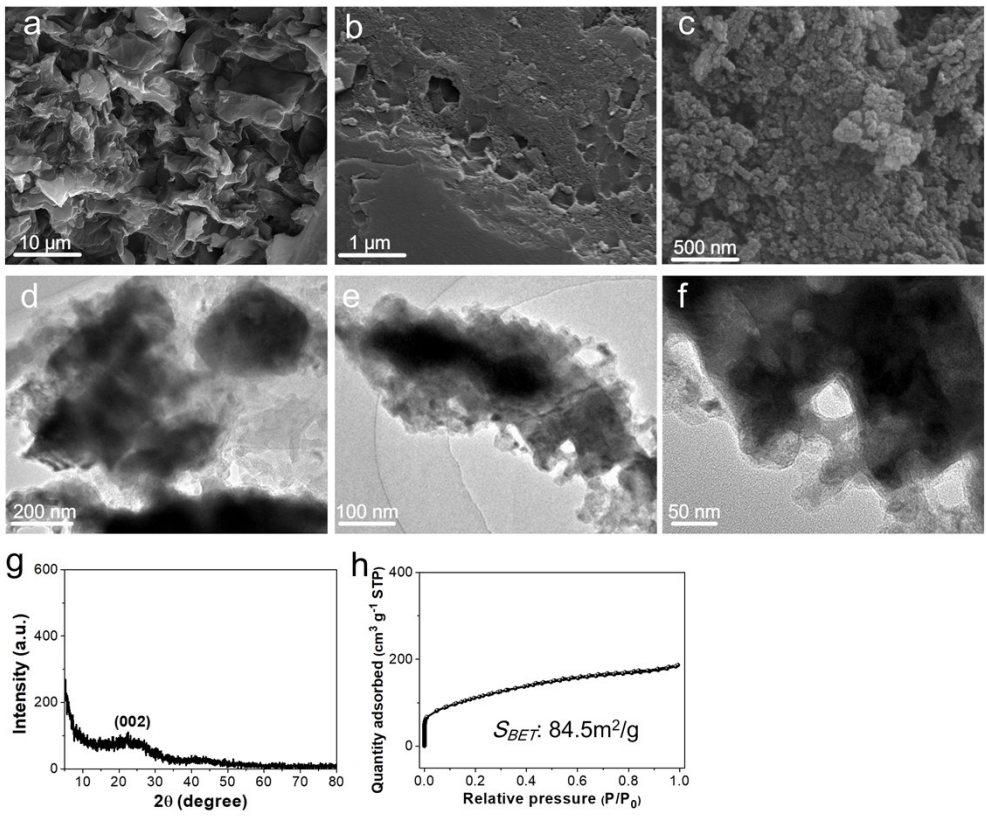

Figure S6 (a-c) SEM images, (d-f) TEM images, (g) XRD pattern and (h) nitrogen adsorption/desorption isotherm of the carbon synthesized without using potassium ferrate.

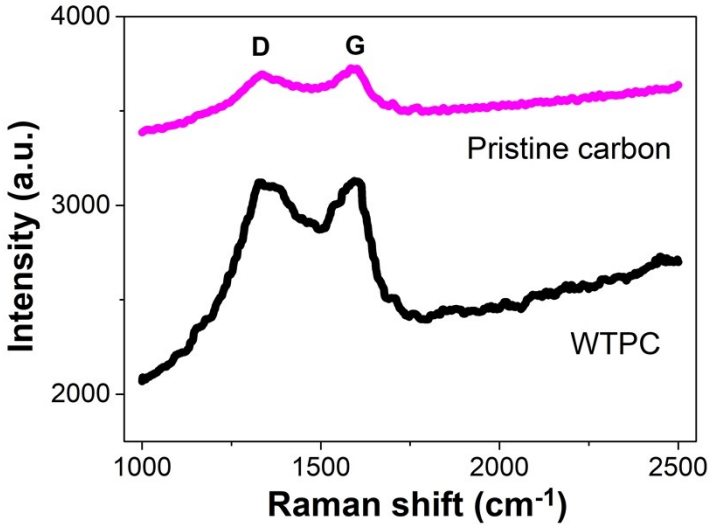

Figure S7 Raman spectra of the pristine carbon synthesized without using potassium ferrate and WTPC.

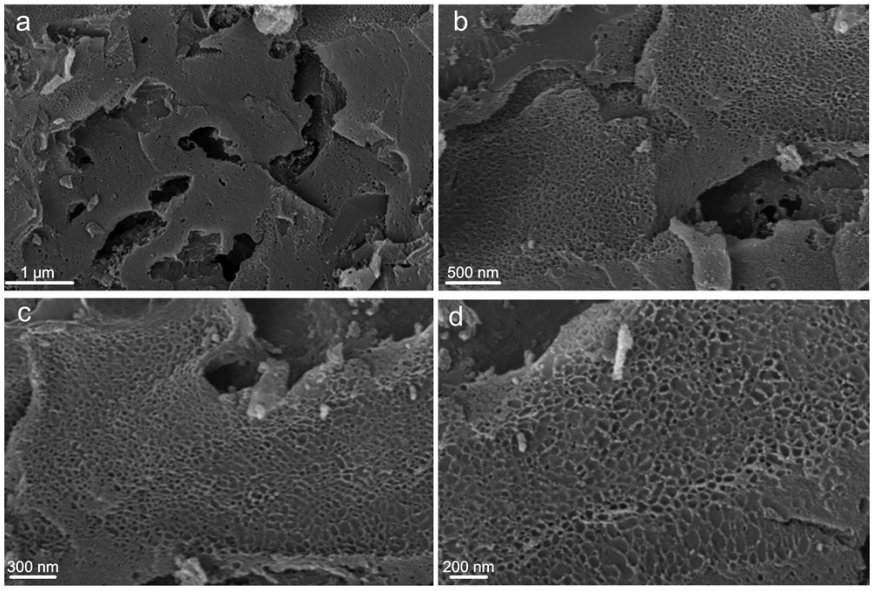

Figure S8 SEM images of WTPC electrode at different magnifications after long-term cycles (a-d).

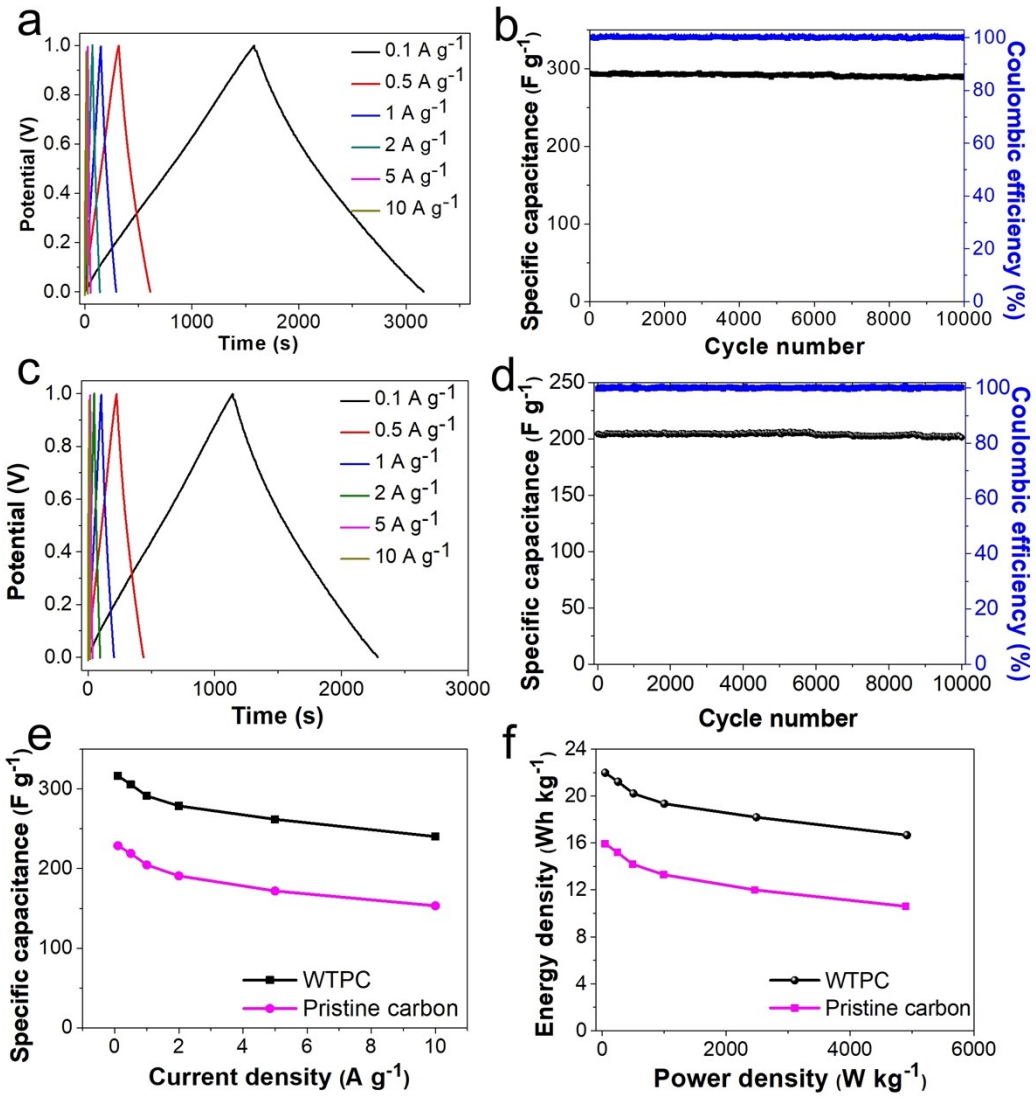

Figure S9 (a) GCD curves and (b) cyclic property (1 A g^{-1}) and Coulombic efficiency of WTPC supercapacitors; (c) GCD curves and (d) cyclic property (1 A g^{-1}) and Coulombic efficiency of pristine carbon supercapacitors; (e) Specific capacitances at different current densities of WTPC and pristine carbon supercapacitors, and (f) Ragone plots of WTPC supercapacitors and pristine carbon supercapacitors.

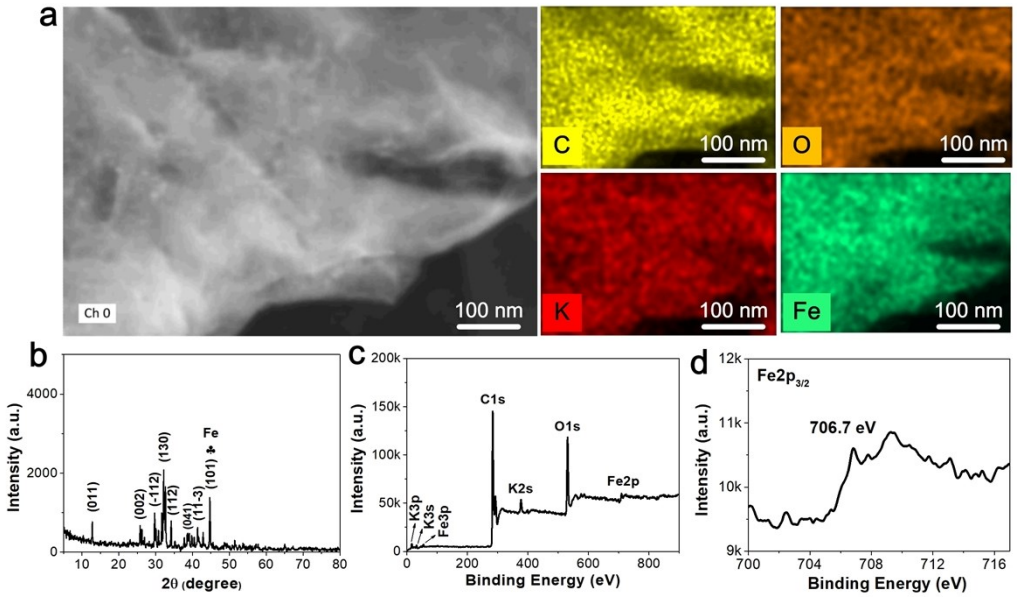

Figure S10 (a) EDS mappings, (b) XRD pattern, (c) survey scan and (d) Fe2p high resolution XPS spectrum of the annealed samples before washing by hydrochloric acid.

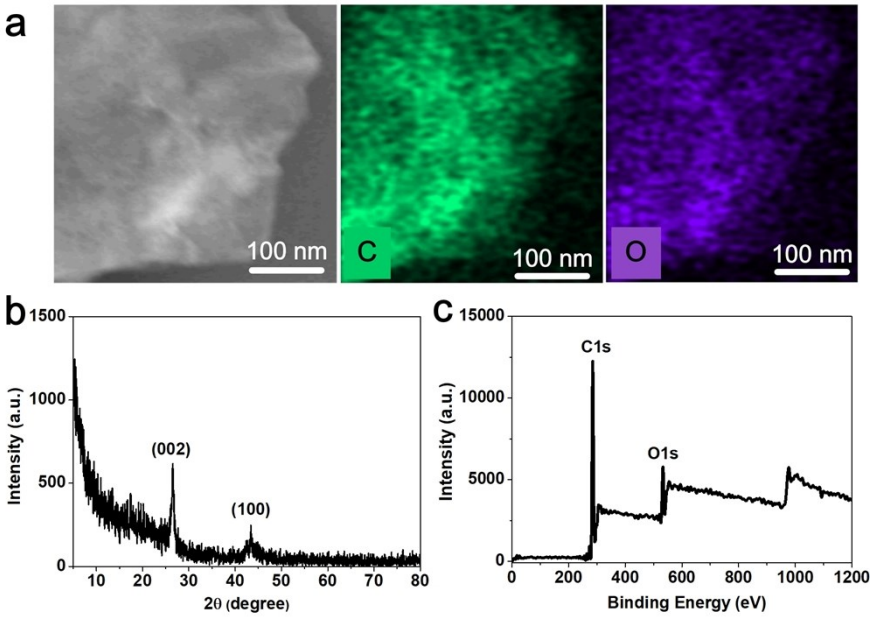

Figure S11 (a) EDS mappings, (b) XRD pattern and (c) XPS spectrum of the annealed samples after washing by hydrochloric acid.

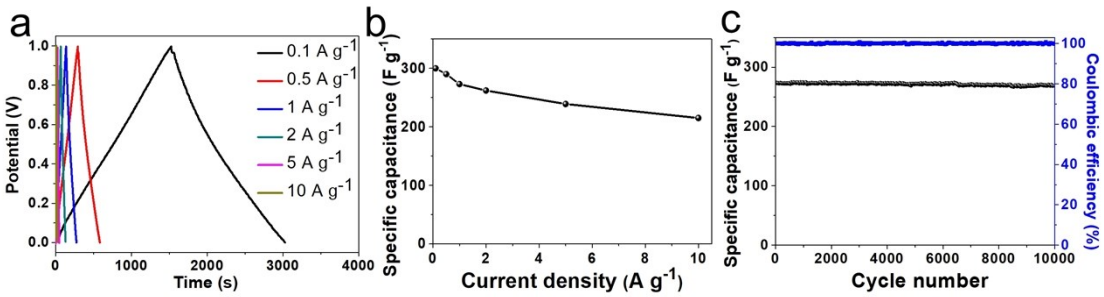

Figure S12 (a) GCD curves, (b) specific capacitances at different current densities, and (c) cyclic property (1 A g^{-1}) and Coulombic efficiency of the WTPC-1 device.

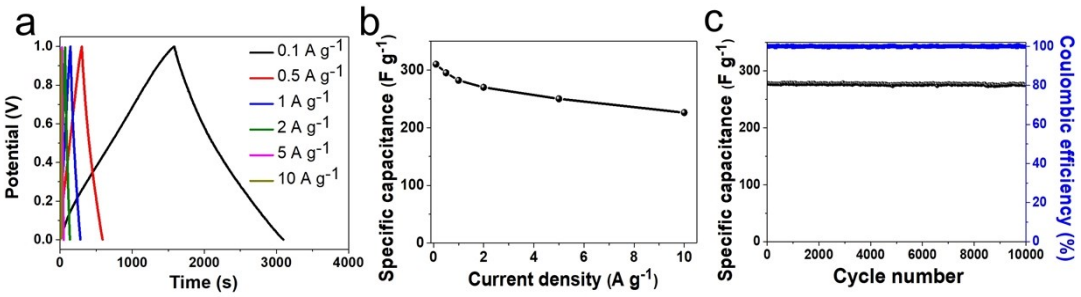

Figure S13 (a) GCD curves, (b) specific capacitances at different current densities and (c) cyclic property (1 A g^{-1}) and Coulombic efficiency of the WTPC-2 device.

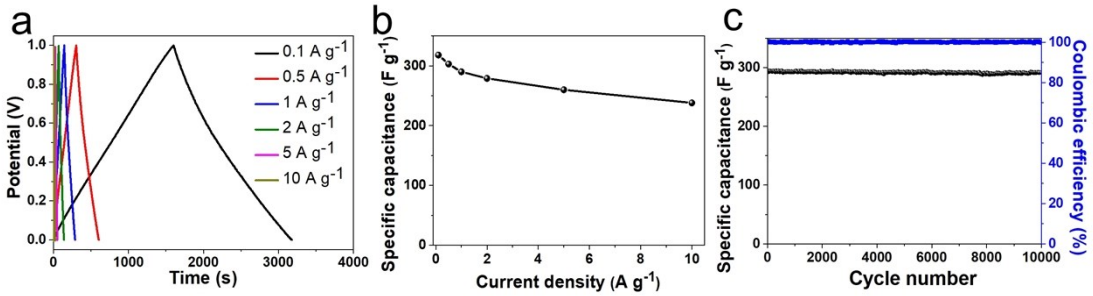

Figure S14 (a) GCD curves, (b) specific capacitances at different current densities and (c) cyclic property (1 A g^{-1}) and Coulombic efficiency of the WTPC-4 device.